# Progressive Supranuclear Palsy: High-Field-Strength MR Microscopy in the Human Substantia Nigra and Globus Pallidus[1]

Parastou Foroutan, MS
Melissa E. Murray, PhD
Shinsuke Fujioka, MD
Katherine J. Schweitzer, MD
Dennis W. Dickson, MD
Zbigniew K. Wszolek, MD
Samuel C. Grant, PhD

**Purpose:** To characterize changes in the magnetic resonance (MR) relaxation properties of progressive supranuclear palsy (PSP) and tissue from neurologically normal brains by using high-resolution (21.1-T, 900-MHz) MR microscopy of postmortem human midbrain and basal ganglia.

**Materials and Methods:** This HIPAA-compliant study was approved by the institutional review board at the Mayo Clinic and informed consent was obtained. Postmortem tissue from age-matched PSP ($n$ = 6) and control ($n$ = 3) brains was imaged by using three-dimensional fast low-angle shot MR imaging with isotropic resolution of 50 μm. Relaxation times and parametric relaxation maps were generated from spin-echo and gradient-recalled-echo sequences. MR findings were correlated with histologic features by evaluating the presence of iron by using Prussian blue and ferritin and microglia burden as determined by a custom-designed color deconvolution algorithm. T2 and T2*, signal intensities, percent pixels (that could not be fitted in a pixel-by-pixel regression analysis due to severe hypointensity), and histologic data (total iron, ferritin, and microglia burden) were statistically analyzed by using independent sample $t$ tests ($P < .05$).

**Results:** PSP specimens showed higher iron burden in the cerebral peduncles and substantia nigra than did controls. However, only the putamen was significantly different, and it correlated with a decrease of T2* compared with controls (−48%; $P$ = .043). Similarly, substantia nigra showed a significant decrease of T2* signal in PSP compared with controls (−57%; $P$ = .028). Compared with controls, cerebral peduncles showed increased T2 (38%; $P$ = .026) and T2* (34%; $P$ = .014), as well as higher T2 signal intensity (57%; $P$ = .049). Ferritin immunoreactivity was the opposite from iron burden and was significantly lower compared with controls in the putamen (−74%; $P$ = .025), red nucleus (−61%; $P$ = .018), and entire basal ganglia section (−63%; $P$ = .016).

**Conclusion:** High-field-strength MR microscopy yielded pronounced differences in substantia nigra and globus pallidus of PSP compared with control brains. Histologic data also suggested that the predominant iron in PSP is hemosiderin, not ferritin. Iron in the brain is a contrast enhancer and potential biomarker for PSP.



[1] From the Department of Chemical & Biomedical Engineering, Florida State University Florida A&M University–Florida State University College of Engineering and National High Magnetic Field Laboratory, 1800 E Paul Dirac Dr, Tallahassee, FL 32310 (P.F., S.C.G.); Department of Pathology and Neuroscience (M.E.M., D.W.D.) and Department of Neurology (S.F., K.J.S., Z.K.W.), Mayo Clinic, Jacksonville, Fla. Received December 9, 2010; revision requested January 26, 2011; revision received July 28; accepted August 23; final version accepted July 24, 2012. K.J.S. supported by German Research Foundation (DFG) and Mayo Clinic Florida Robert and Clarice Smith Fellowship. D.W.D. supported by National Institutes of Health (NIH) (P50-AG25711, P50-AG16574, P50-NS40256, P01-AG17216, P01-AG03949, and R01-AG15866). Z.K.W. supported by Mayo Clinic Florida Research Committee CR program (MCF #90052018 and MCF #90052030); NIH [NINDS 1RC2NS070276, P50NS057567, P50NS072187]; and a gift from Carl Edward Bolch, Jr, and Susan Bass Bolch (MCF #90052031/PAU #90052). S.C.G. supported by National Science Foundation (DMR 0084173) and Florida State University. **Address correspondence to** S.C.G. (e-mail: *parastou.foroutan@moffitt.org*).

Progressive supranuclear palsy (PSP), also known as Richardson-Steele-Olszewski syndrome, is the second most common form of neurodegenerative parkinsonism (1), with an estimated prevalence of one to five cases per 100000 (2). Clinical characteristics of PSP include axial rigidity, vertical gaze palsy, and frequent falls; these symptoms begin early in the disease course. Subcortical dementia develops in later stages of PSP (3–5). PSP is associated with neuronal cell loss in cortical and subcortical structures, including the substantia nigra, globus pallidus, and subthalamic nucleus (6).

There has been great progress in the clinical assessment of neurodegenerative disorders, including PSP, with the use of magnetic resonance (MR) imaging (1,7). However, the definitive diagnosis of these various degenerative conditions still must be confirmed with postmortem examination. Compared with in vivo MR imaging assessment, postmortem MR imaging of human brain tissue offers several advantages, including the possibility to acquire higher resolution over longer acquisition times while preserving the tissue for histologic correlative analyses. With histologic specimens, MR microscopy at ultrahigh magnetic field strength (eg, 21.1 T) provides the sensitivity required to visualize and measure potential biomarkers and relaxation parameters that may be related to neurodegeneration. As such, these investigations may provide insight not only into underlying pathologic conditions, but they may also inform future diagnostic evaluations of these diseases. To characterize changes in MR relaxation properties of PSP compared with tissue from neurologically healthy subjects, high-resolution MR microscopy of postmortem human basal ganglia and midbrain was acquired at 21.1 T (900 MHz).

## Advances in Knowledge

- High-field-strength (21.1-T) MR microscopy demonstrated changes in the substructures of the substantia nigra and globus pallidus in patients with progressive supranuclear palsy (PSP), as reflected by decreases in T2 and T2*.
- These changes in the substructures of the substantia nigra and globus pallidus were correlated with iron deposits that were confirmed at histologic analysis in these regions.

## Materials and Methods

This Health Insurance Portability and Accountability Act–compliant study was approved by the Mayo Clinic's institutional review board and was performed between May 2009 and October 2010. Informed consent was obtained from legal next of kin for all autopsies. Postmortem tissue was selected at the time of gross examination from a consecutive series of autopsied brains from the Mayo Clinic brain bank in Jacksonville, Florida. Of the 28 brains that underwent MR microscopy imaging, 13 were excluded because of a pathologic diagnosis of Lewy body disease (8). Three of the 10 PSP cases were excluded for neuropathologic features of atypical PSP, based on τ immunohistochemistry (D.W.D., over 25 years experience with neuropathologic evaluation and diagnosis) or poor-quality tissue samples with either excessive fixation or postmortem handling artifacts. The control series ($n$ = 5) was selected from 28 cases that were processed at the same time, met the same tissue quality criteria as for PSP brains, and were free of disease processes at neuropathologic evaluations (D.W.D.). From the PSP ($n$ = 6) and control ($n$ = 5) brains that remained, available medical records were reviewed (S.F. and K.J.S., over 10 years of experience in neurology). A clinical diagnosis of PSP was confirmed in all cases (3); however, two of the controls were excluded because of an antemortem diagnosis of dementia with Lewy body disease (9) and vascular dementia (10). The PSP samples were from the CurePSP/Society for Progressive Supranuclear Palsy Brain Bank (11). Samples of the basal ganglia were obtained from six women (age range, 68–81 years; mean, 76 years ± 6 [standard deviation]) with pathologically confirmed PSP (12) and three neurologically healthy women of similar age (range, 65–73 years; mean, 70 years ± 4). The fixed-tissue specimens were placed in plastic tissue cassettes (Triangle Biomedical Sciences, Durham, NC) and maintained at 4°C until MR microscopy evaluation (P.F., 6 years of experience in MR imaging; S.C.G., 16 years in MR susceptibility matching). Prior to MR imaging, the samples were washed in phosphate-buffered saline and immersed in liquid coolant (Fluorinert FC-43; 3M, Minneapolis, Minn) at room temperature (21°–23°C) for 45 minutes to remove air bubbles from the surfaces and crevasses of the tissue (13).

All MR data were acquired by two of the authors (P.F., S.C.G.) using a 21.1-T ultra–wide bore (105-mm) vertical magnet that was equipped with an Avance III (Bruker, Madison, Wis) console and specially built, 1 T/m/A three-axes gradient system (Resonance Research, Billerica, Mass) that had a diameter of 64 mm. By utilizing a 33-mm birdcage coil,

**Published online before print**
10.1148/radiol.12102273 **Content code:** MR

**Radiology 2013;** 266:280–288

**Abbreviations:**
FLASH = fast low-angle shot
PSP = progressive supranuclear palsy
ROI = regions of interest
SI = signal intensity
TE = echo time
TR = repetition time

**Author contributions:**
Guarantors of integrity of entire study, P.F., K.J.S., Z.K.W., S.C.G.; study concepts/study design or data acquisition or data analysis/interpretation, all authors; manuscript drafting or manuscript revision for important intellectual content, all authors; approval of final version of submitted manuscript, all authors; literature research, K.J.S., D.W.D., S.C.G.; clinical studies, S.F., D.W.D., Z.K.W., S.C.G.; experimental studies, P.F., M.E.M., K.J.S., Z.K.W., S.C.G.; statistical analysis, P.F., S.F., D.W.D., S.C.G.; and manuscript editing, P.F., M.E.M., K.J.S., D.W.D., Z.K.W., S.C.G.

**Funding:**
This research was supported by the National Institutes of Health (grants P50-AG25711, P50-AG16574, P50-NS40256, P01-AG17216, P01-AG03949, R01-AG15866, NINDS 1RC2NS070276, P50NS057567, and P50NS072187).

Conflicts of interest are listed at the end of this article.

three-dimensional fast low-angle shot (FLASH) gradient-recalled-echo images (echo time [TE] msec/repetition time [TR] msec, 4/50) were acquired at the isotropic resolution of 50 μm during 4.3 hours at 14°C. In addition, T2*-weighted multiple gradient-recalled-echo and T2-weighted spin-echo sequences were performed over a range of TEs (TE = 3.5–45.4 msec and TE = 7.9–94.8 msec, respectively) to generate quantitative relaxation maps. Spatial resolution for these images was 100 × 100 × 550 μm. To provide a visual assessment of midbrain and basal ganglia microstructural border delineation, we consulted the neuroanatomy atlas by Haines (14). For quantitative analysis of T2, T2*, and signal intensity (SI), regions of interest (ROIs) were traced over the entire cerebral peduncles, substantia nigra, and red nucleus in the midbrain section. For the basal ganglia, ROIs were positioned to individually encompass the entire globus pallidus interna, globus pallidus externa, and putamen (P.F., S.C.G.). To calculate T2 and T2* values over these ROIs, average SIs for all sampled TEs were fitted to a three-parameter single exponential decay function by using a Levenberg-Marquardt nonlinear regression analysis. To visualize the disparity between T2*- and T2-based contrast, quantitative parametric relaxation maps were generated on a pixel-by-pixel basis by means of a nonlinear regression of the pixel SI. By applying a 90% threshold to the parametric relaxation maps, the ratio of hyperintense T2 and T2* pixels to the total number of pixels in each ROI was quantified. In addition, histograms of the SI for the lowest-weighted T2- and T2*-weighted images also were plotted to evaluate signal distribution over the entire specimen (P.F., S.C.G.).

Subsequent to MR imaging, the tissue was processed for paraffin embedding, and 5-μm-thick sections were cut for histologic studies. Prussian blue stain was used to detect iron. This stain uses a 20% aqueous solution of hydrochloric acid and 10% aqueous solution of potassium ferrocyanide that reacts with ferric iron to produce an insoluble blue compound, ferric ferrocyanide (15). Nuclear fast red dye was used as a counterstain. The sections also were immunostained for ferritin and microglia by using an L-ferritin polyclonal antibody (ab69090; Abcam, Cambridge, Mass) and a monoclonal antibody to the ionized calcium-binding adaptor molecule 1 (Iba1; Wako Chemicals, Richmond, Va), respectively. Stained slides were scanned on an automated, high-throughput slide scanner (ScanScope XT; Aperio, Vista, Calif) and analyzed with ImageScope software (Aperio) (M.E.M., digital microscopy expertise with 5 years of experience in annotation and algorithm design with the Aperio system). Three-color deconvolution algorithms were customized to the specific optical density of the Prussian blue deposits, ferritin-positive structures, and Iba1-positive microglia (M.E.M.). The output for each algorithm was a percentage burden that represented the positively stained area out of the total area annotated for each ROI. To coregister ROIs between MR images and histologic slides, a dual-monitor system was used to display both the three-dimensional FLASH image and the corresponding histologic image of the Prussian blue–stained tissue, and the same ROI borders were drawn for all structures (P.F., M.E.M.).

For the comparison of relaxation times, SI, pixel dropouts, and histologic data, statistical analyses were performed (by P.F., S.C.G.) by analyzing independent samples *t* tests (SPSS 16.0 for Windows; SPSS, Chicago, Ill). Statistical significance was predetermined at $P < .05$.

## Results

The high-resolution FLASH data sets allowed depiction of microstructural details of both basal ganglia and midbrain structures in normal control brains, with microstructure borders delineated in neurologically normal brains (Figs 1a, 2a) than in PSP (Figs 3a, 4a).

Demonstrated by the parametric relaxation data, the T2* maps (Figs 1b, 2b, 3b, 4b) and, to a lesser extent, the T2 maps of the PSP specimen showed clusters of hyperintense regions (ie, white areas) that correspond to the darker areas in the three-dimensional data set (Figs 1a, 2a, 3a, 4a). These hyperintense regions demarcated pixels that could not be fitted as part of the pixel-by-pixel regression for T2* because the TE signals that were greater than 10 msec could not be distinguished from baseline noise. Not surprisingly, some of these same regions demonstrated similar dropout for the T2 regression analysis. The ratio of hyperintense T2* to T2 pixels (overlaid pixels in Figs 3 and 4b) to the total number of pixels in the same ROI displayed larger values for the PSP samples than for the controls for all regions except for the red nucleus ($P = .704$) and cerebral peduncles ($P = .292$). In agreement with relaxation data, hyperintense T2*-weighted pixels in the putamen were significantly increased ($P = .008$) in PSP compared with controls (Table 1).

As shown in Table 2, there was a trend toward lower T2 and T2* values for all ROIs in the globus pallidus of PSP-affected brains compared with controls. This trend was more prominent for T2*, which underwent a significant decrease (34%; $P = .043$) in the putamen. Although the differences in T2 between PSP and control brains were smaller and were not statistically significant, the putamen underwent a decrease of 21% ($P = .102$), which was the largest decrease among the other substructures. These results corroborated the outcome of the visual analysis of both MR images and quantitative parametric relaxation maps and also quantitatively demonstrated the large and differential alteration of subregions in the globus pallidus in PSP brains compared with controls. Similar to the globus pallidus, the midbrain in PSP demonstrated nonsignificant decreases in T2* for the substantia nigra (−14%; $P = .827$) and red nucleus (−15%, $P = .687$), while the cerebral peduncles demonstrated the opposite trend with a significant increase of T2* (26%; $P = .014$). Interestingly, T2 was also higher for the cerebral peduncles, which underwent a significant increase (27%; $P = .026$).

As expected, owing to information obtained from the quantitative parametric relaxation maps, SI was relatively

**Figure 1**

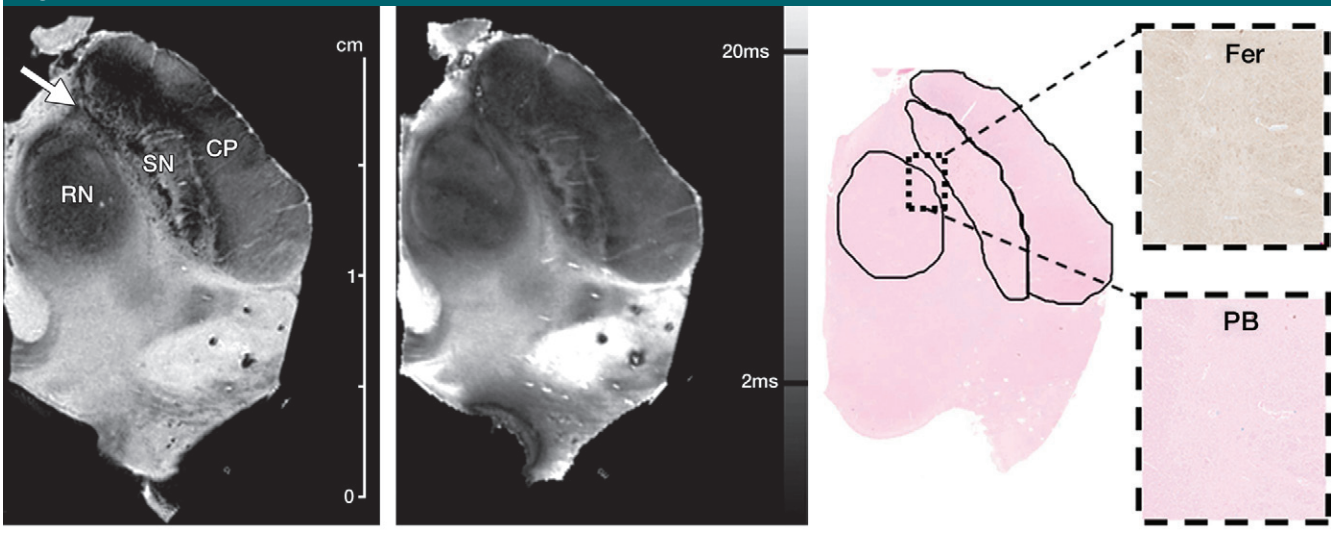


**Figure 1:** Normal control midbrain specimen of a 73-year-old woman. **(a)** Three-dimensional FLASH MR imaging partitions (4/50; isotropic resolution, 50 μm; acquisition time, 4.3 h) acquired at 21.1 T (900 MHz). Arrow = delineation between substantia nigra *(SN)* and red nucleus *(RN)*. *CP* = cerebral peduncles. **(b)** Parametric relaxation map shows T2* contribution, as well as range in T2* times. **(c)** Histologic regions of the control tissue with Prussian blue *(PB)* stain and L-ferritin *(Fer)* immunohistochemistry demonstrate lack of iron in control midbrain, which coincides with normal signal intensity on T2*-weighted images and relaxation maps in PSP brains. (Outset images magnification, ×4.)

**Figure 2**

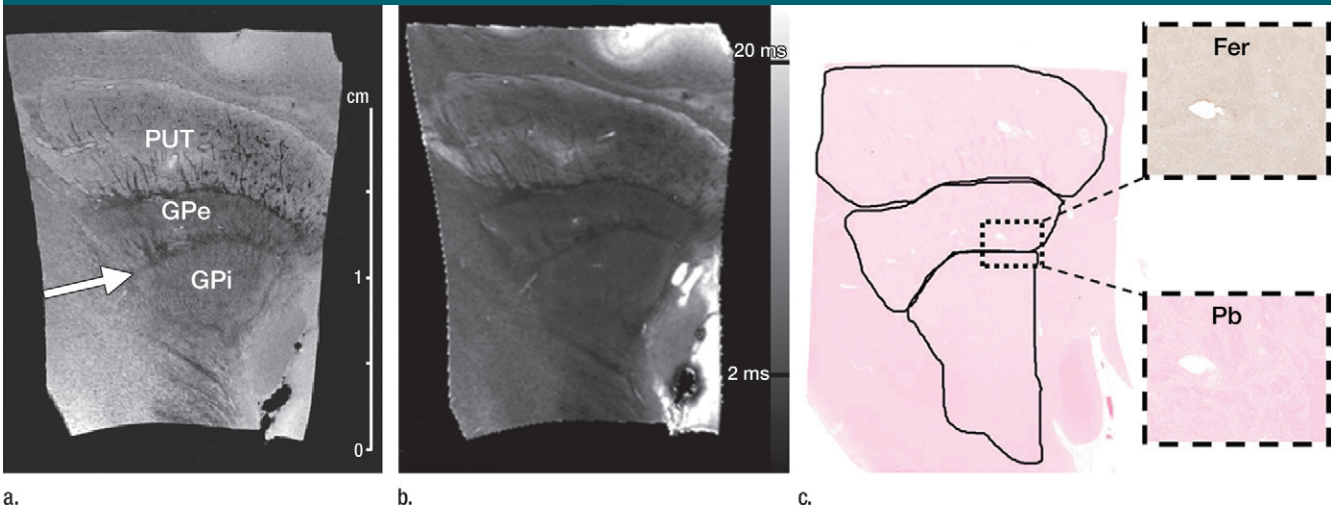


**Figure 2:** Normal control globus pallidus of a 73-year-old woman. **(a)** Three-dimensional FLASH MR imaging partitions (4/50; isotropic resolution, 50 μm; acquisition time, 4.3 h). Arrow = delineation between globus pallidus interna *(GPi)* and externa *(GPe)*. *Put* = putamen. **(b)** Parametric relaxation map that shows T2* contributions as well as ranges in T2* times. **(c)** Prussian blue *(Pb)* staining and L-ferritin *(Fer)* immunohistochemistry demonstrated nonsignificant macroscopic and microscopic differences in the normal control specimen. (Outset images magnification, ×4.)

similar across groups regarding T2. However, the SI in the cerebral peduncles of controls was significantly increased (57%; $P = .049$) compared with the PSP cases (Table 2), which thereby corroborated the relaxation data. In addition, the T2*-based SI demonstrated significantly lower values (57%; $P = .028$) for the substantia nigra in PSP brains compared with controls.

The results of the histologic analysis of iron with Prussian blue stain and L-ferritin to characterize the major iron binding protein in the brain and ferric iron are respectively demonstrated in

**Figure 3**

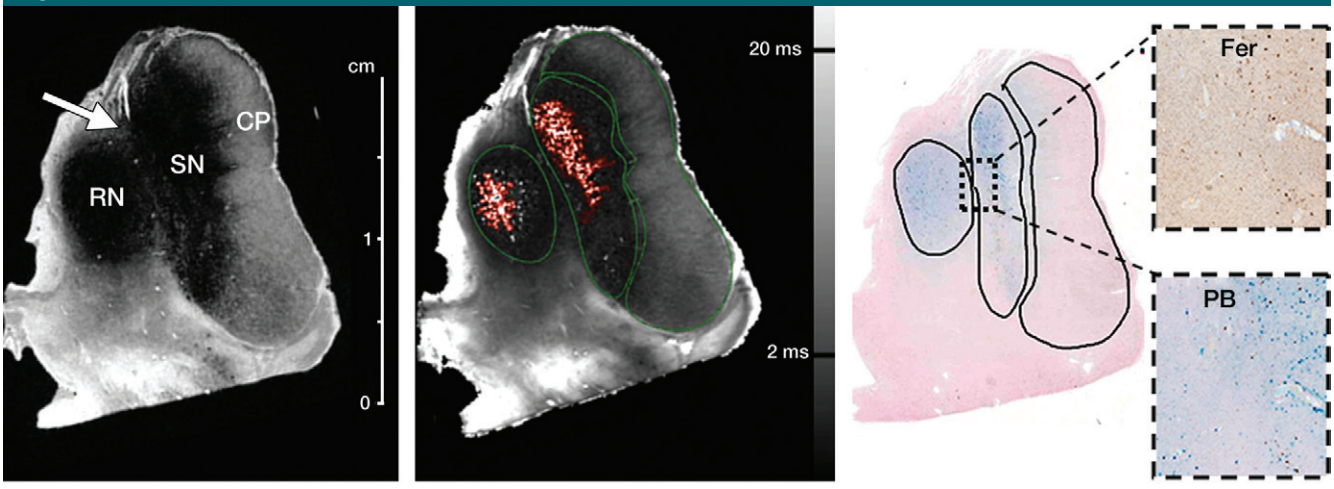


**Figure 3:** PSP midbrain specimen of a 70-year-old woman. **(a)** Three-dimensional FLASH MR imaging partitions (4/50; isotropic resolution, 50 μm; acquisition time, 4.3 h) acquired at 21.1 T (900 MHz). Arrow = hypointense pixels of red nucleus *(RN)* that adjoin those of substantia nigra *(SN)* and shows less delineation between structures. *CP* = cerebral peduncles. **(b)** T2*-weighted map that shows manually drawn ROIs and pixel dropouts (overlaid in orange) that could not be fitted as part of pixel-by-pixel regression. **(c)** Histologic analysis of tissue with Prussian blue *(PB)* stain and L-ferritin *(Fer)* immunohistochemistry reveal iron deposits that coincide with abnormal signal intensity on T2*-weighted images and relaxation maps in PSP brains. (Outset images magnification, ×4.)

**Figure 4**

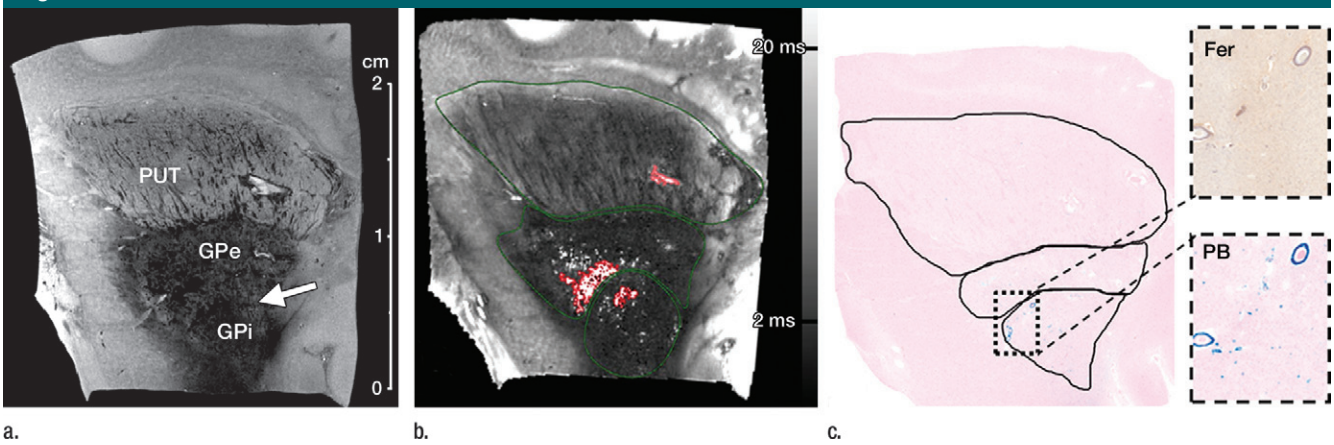


**Figure 4:** PSP globus pallidus of a 68-year-old woman. **(a)** Three-dimensional FLASH MR image (4/50; isotropic resolution, 50 μm; acquisition time, 4.3 h). Arrow = hypointense pixels of the globus pallidus interna *(GPi)* that adjoins those of globus pallidus externa *(GPe)*. Note lack of clearly identifiable border. **(b)** T2*-weighted map displays manually drawn ROIs and pixel dropouts (overlaid in orange) that could not be fitted as part of pixel-by-pixel regression. **(c)** Histologic slide of tissue with Prussian blue *(PB)* stain and L-ferritin *(Fer)* immunohistochemistry reveal iron deposits that coincide with abnormal signal intensity on T2*-weighted images and relaxation maps for the pathologic specimen. (Outset images magnification, ×4.)

Figures 1c, 2c, 3c, and 4c and in Table 3. While PSP specimens had an iron burden that ranged from 31% ($P$ = .571) for the cerebral peduncles to 426% ($P$ = .217) for the substantia nigra and was higher than that in controls, only the putamen iron content had a statistically significant change, with a 307% ($P$ = .005) increase that correlated with a significant decrease of T2* (−48%; $P$ = .043). Similarly, the substantia nigra demonstrated a significant decrease of T2* signal in PSP compared with that in controls (−57%; $P$ = .028). Interestingly, the cerebral peduncles demonstrated increased T2 (38%; $P$ = .026) and T2* (34%; $P$ = .014), as well as higher T2 SI (57%; $P$ = .049). Ferritin demonstrated a trend that was opposite to that of the iron burden, and its immunoreactivity was significantly lower in the putamen (−74%; $P$ = .025), red nucleus (−61%; $P$ = .018), and the entire basal ganglia section (−63%;

$P$ = .016). In addition, quantitative image analysis of Iba1 immunoreactivity for microglia showed increases in PSP compared with controls (105% in the putamen; $P$ = .295), but in no region was the increase statistically significant.

**Table 1**

**Percentage of Pixels per Region that did not Fit in a Pixel-by-Pixel Regression due to Severe Hypointensity**

| | Control Brains | | PSP Brains | |
|---|---|---|---|---|
| ROI | T2 Pixels (%) | T2* Pixels (%) | T2 Pixels (%) | T2* Pixels (%) |
| SN | 1.2 ± 1.1 | 1.8 ± 0.0 | 3.4 ± 2.1 (.078) | 2.6 ± 1.9 (.627) |
| RN | 0.8 ± 1.4 | 1.3 ± 0.0 | 0.8 ± 1.9 (.970) | 0.8 ± 1.8 (.704) |
| CP | 1.1 ± 1.5 | 2.5 ± 0.7 | 2.4 ± 2.0 (.316) | 0.9 ± 1.0 (.292) |
| GPi | 0.2 ± 0.4 | 0.8 ± 1.4 | 3.4 ± 2.6 (.051) | 2.7 ± 1.9 (.109) |
| GPe | 1.8 ± 2.0 | 2.2 ± 0.4 | 3.1 ± 1.5 (.340) | 2.9 ± 1.7 (.589) |
| Put | 3.2 ± 1.1 | 2.7 ± 1.4* | 3.7 ± 2.0 (.621) | 6.1 ± 0.4 (.008)* |

Note.—CP = cerebral peduncles, GPe = globus pallidus externa, GPi = globus pallidus interna, Put = putamen, RN = red nucleus, SN = substantia nigra. Numbers in parentheses are $P$ values.

* Indicates significant difference in an independent sample $t$ test ($P < .05$) between PSP and control specimen.

## Discussion

By quantifying MR imaging contrast and relaxation in fixed-tissue specimens and by correlating these observations with the levels of ferric iron, L-ferritin, and microglia with image analysis in the same tissue samples, we found that high-field-strength MR microscopy with high resolution at 21.1 T demonstrated pronounced differences in the substantia nigra and globus pallidus of PSP brains compared with neurologically normal control brains. These results demonstrated the ability of high-resolution MR microscopy at high magnetic field strength to show visual changes in PSP compared with normal brain tissue.

Even though the 21.1-T system used in this study is at the extreme end of the high field strengths that are currently available for MR imaging, other lower magnetic field strengths have been used to help evaluate neurodegeneration in pathologic specimens, particularly for Alzheimer disease (16,17). Additionally, there is strong potential that these techniques could be translated to clinical field strengths, as indicated by Meadowcroft et al (18), which underscores the potential for correlative MR imaging–based pathologic evaluations and the prospect for translation to diagnostic imaging in the differential diagnoses of parkinsonian disorders. Interestingly, previous in vivo MR imaging studies have focused on morphometric analyses to quantify atrophy in the midbrain, pons, and cerebellar peduncles and to differentiate PSP from other movement disorders (7,19). Though these morphometric techniques have good sensitivity, the relaxation-based approach utilized here may provide novel indices that will improve diagnostic imaging of parkinsonism. For example, two recent studies (20,21) have correlated lower T2 and T2* values for patients with Parkinson disease in the substantia nigra and putamen, with correlations to biochemical assay results from other postmortem studies of brain iron (22,23). These approaches indicate a positive correlation between clinical MR imaging and ex vivo iron analysis that could equally be applied to PSP. Furthermore, the commonalities between MR imaging signal intensity decreases and iron deposition in both PSP and Parkinson disease may indicate a similar pathogenesis, although further work must be conducted to examine the role of iron and its utility in classification of parkinsonian disorders.

Compared with the surrounding tissue and controls, high-resolution three-dimensional datasets and parametric relaxation maps displayed darker substantia nigra and globus pallidus with shorter T2 and T2* in PSP. While the darker areas in the pathologic images may appear to facilitate the detection of each region, the delineation of structures as well as anatomic subregions within these structures was more pronounced in controls than in PSP. The hypointensity in PSP has been reported in previous studies; however, it has not been quantified in any manner, and although it has been speculated that iron may play a role, the source of the darker areas has not yet been investigated (24,25). In addition to the high-resolution three-dimensional images that allowed for an in-depth visual analysis of the fine structural details in these regions, the quantitative parametric relaxation maps more clearly showed the impact of each contrast mechanism (ie, T1, T2, and T2*). As expected at higher magnetic field strength, these maps demonstrated that the majority of contrast viewed in these anatomic images was based on T2* and, to a lesser extent, T2. In addition, the T2* maps provided information in the form of pixel dropouts that represented regions of strong hypointensity and that could not be distinguished from the surrounding noise. Quantitative analysis of these pixels showed more dropouts in PSP brains than in controls, and this was corroborated by the histologic data that showed significant increases in Prussian blue–stained iron. These results indicated that these areas may be of particular importance in the differentiation of PSP specimens from controls and should be evaluated further.

Previously, a wide range of postmortem biochemical studies found increased iron content in the parkinsonian substantia nigra (26–28), globus pallidus (29), dentate nucleus (30), caudate nucleus, and putamen (31) compared with iron content in normal control tissue. Furthermore, iron accumulation has been shown to correlate with disease severity (32). Excess iron may favor generation of reactive oxygen species, which could lead to neuronal

**Table 2**

**Average Absolute T2 and T2* Times with Corresponding SIs for the PSP Group versus the Control Group**

| | Control Brains | | | | PSP Brains* | | | |
|---|---|---|---|---|---|---|---|---|
| ROI | T2 (msec) | T2* (msec) | T2-based SI | T2*-based SI | T2 (msec) | T2* (msec) | T2-based SI | T2*-based SI |
| SN | 18.4 ± 4.1 | 5.3 ± 1.1 | 1.0 ± 0.2 | 9.8 ± 4.5† | 19.8 ± 8.2 (.737) | 5.0 ± 3.2 (.827) | 0.9 ± 0.2 (.531) | 4.2 ± 1.8 (.028)† |
| RN | 17.9 ± 5.2 | 6.4 ± 2.1 | 0.8 ± 0.2 | 10.3 ± 4.5 | 21.7 ± 8.3 (.427) | 5.7 ± 3.0 (.687) | 0.9 ± 0.2 (.438) | 6.0 ± 1.5 (.060) |
| CP | 21.9 ± 2.3† | 5.8 ± 0.5† | 0.7 ± 0.2† | 9.2 ± 3.8 | 30.3 ± 6.5 (.026)† | 7.8 ± 1.3 (.014)† | 1.1 ± 0.3 (.049)† | 5.7 ± 2.2 (.117) |
| GPi | 16.7 ± 4.8 | 4.9 ± 1.8 | 0.6 ± 0.2 | 3.0 ± 1.1 | 15.1 ± 5.8 (.682) | 3.5 ± 1.0 (.164) | 0.6 ± 0.1 (.922) | 3.8 ± 1.1 (.317) |
| GPe | 18.4 ± 4.2 | 5.6 ± 2.1 | 0.7 ± 0.2 | 3.5 ± 1.5 | 15.4 ± 5.2 (.394) | 3.9 ± 0.8 (.104) | 0.6 ± 0.1 (.400) | 3.9 ± 1.0 (.660) |
| Put | 24.2 ± 3.3 | 10.2 ± 2.3† | 0.8 ± 0.2 | 4.3 ± 1.7 | 18.9 ± 5.0 (.102) | 6.9 ± 1.6† (.043) | 0.8 ± 0.1 (.866) | 5.6 ± 1.7 (.328) |

Note.—CP = cerebral peduncles, GPe = globus pallidus externa, GPi = globus pallidus interna, Put = putamen, RN = red nucleus, SN = substantia nigra.

* Numbers in parentheses are *P* values.

† Indicates significant difference in an independent sample *t* test ($P < .05$) between PSP and control specimen.

**Table 3**

**Burden of Total Iron, Ferritin, and Microglia Obtained after Histologic Staining**

| | Control Brains | | | PSP Brains | | |
|---|---|---|---|---|---|---|
| ROI | Burden (%) | Ferritin (%) | Iba-1 (%) | Burden (%) | Ferritin (%) | Iba-1 (%) |
| SN | 0.28 ± 0.16 | 3.33 ± 1.08 | 3.39 ± 1.05 | 1.45 ± 1.79 (.217) | 2.61 ± 1.08 (.262) | 5.36 ± 4.27 (.327) |
| RN | 0.15 ± 0.04 | 7.46 ± 3.03* | 2.43 ± 1.72 | 0.29 ± 0.36 (.431) | 2.89 ± 1.90 (.018)* | 4.63 ± 3.30 (.327) |
| CP | 0.13 ± 0.07 | 3.84 ± 2.54 | 4.27 ± 1.35 | 0.17 ± 0.13 (.571) | 4.53 ± 2.34 (.611) | 5.48 ± 2.99 (.430) |
| GPi | 0.23 ± 0.15 | 2.80 ± 1.44 | 2.84 ± 2.44 | 0.56 ± 0.57 (.283) | 1.99 ± 0.78 (.330) | 3.67 ± 2.64 (.670) |
| GPe | 0.18 ± 0.11 | 3.19 ± 1.27 | 1.63 ± 1.66 | 0.42 ± 0.42 (.287) | 1.98 ± 0.70 (.124) | 2.20 ± 2.25 (.700) |
| Put | 0.13 ± 0.07* | 6.83 ± 3.96* | 0.91 ± 0.50 | 0.25 ± 0.18 (.005)* | 1.77 ± 0.55 (.025)* | 1.86 ± 1.70 (.295) |
| BG | 0.13 ± 0.07 | 4.81 ± 2.01* | 2.19 ± 1.96 | 0.25 ± 0.18 (.264) | 1.78 ± 0.55 (.016)* | 1.52 ± 1.22 (.572) |

Note.— CP = cerebral peduncles, GPe = globus pallidus externa, GPi = globus pallidus interna, Iba-1= microglia, Put = putamen, RN = red nucleus, SN = substantia nigra.

* Indicates significant difference in an independent sample *t* test ($P < .05$) between PSP and control specimen.

degeneration (33). Iron possesses paramagnetic properties that have an effect on relaxation and induce localized susceptibility-based perturbations of the magnetic field. In the current study, the higher iron burden was correlated with loss of T2- and T2*-weighted signal intensity and it reduced relaxation both globally across the entire specimen and differentially in subregions of the substantia nigra and globus pallidus.

While the data showed that there were increases in iron content in PSP, the amount in the iron-storing protein ferritin showed the opposite, with lower burden of L-ferritin immunoreactivity in PSP compared with controls. Total body iron is approximately 27% stored iron, which provides a source of iron when the physiologic demand is high (34). In the human body, the main physiologic iron storage compound is ferritin, while hemosiderin is considered to be a form of iron storage that is associated with pathologic processes. Ferritin acts as a buffer against iron deficiency or overload, and it is the major source of iron for cellular uptake. Ferritin is soluble, dispersed throughout human organs (ie, liver, heart, and brain), and can be rapidly mobilized; hemosiderin appears as insoluble aggregates that are often associated with iron overload or with hemorrhage and situations that are associated with neurodegeneration (35). Unlike ferritin, hemosiderin can be stained with Prussian blue. The histologic data of this work, therefore, corroborates previous findings of increases in brain iron that do not necessarily correlate with increases in ferritin (36), and suggests that the predominant source of iron in PSP is hemosiderin rather than ferritin.

Ferritin in the brain is abundant in glia, and includes oligodendroglia (35) and microglia (37); therefore, it was of interest to determine whether changes in ferritin's immunoreactivity correlated with microglial burden. Immunohistochemistry for Iba1, a sensitive method for detecting microglia (38), was used for this purpose. Iba1-positive microglia increased in all regions in PSP compared with controls, but given the abundance of Iba1-positive microglia in controls, no statistical difference was found. The lack of significant increase in Iba1-positive microglial burden in PSP suggested that the higher local distribution of iron or the enhancement

of MR imaging contrast was not related to microgliosis.

One limitation of our study was its small sample size. Our study was also limited to women, but there was no evidence of sex-based differences in frequency (2) or clinical or pathologic severity of PSP. By providing evidence of differences in two brain regions known to be affected by PSP, we have attempted to alleviate some concern associated with results that were derived simply by chance. Another limitation of our study was the comparison between a cutting-edge MR technology and an iron-staining technique that dates back to the 18th century. However, we used modern immunohistochemical methods for the iron-binding protein L-ferritin and for microglia; we also used histologic quantification with an advanced digital microscopy system. Future studies should explore newer techniques in metal staining to ascertain the extent to which microscopic differences could be used in high-field MR imaging.

In conclusion, MR microscopy at high magnetic field strength provides the sensitivity required to differentiate PSP from normal control brain tissue. However, the exact role of iron in the pathogenesis of neurodegenerative conditions such as PSP is still unclear and needs further investigation. For PSP, nonheme iron protein in the brain serves as a contrast enhancer and as a potential pathologic biomarker in MR imaging studies, and it has the ability to help distinguish PSP from normal controls. Future MR microscopy studies on larger numbers of cases and the comparison of PSP to other parkinsonian disorders should focus on qualitative or quantitative differences that may improve differential diagnosis of these disorders.

**Acknowledgments:** The authors thank Monica Castanedes-Casey (immunohistochemistry, 15 years), Virginia Phillips (tissue preparation and histologic sectioning, 25 years) and Linda Rousseau (tissue preparation and histologic sectioning, special stain, Prussian blue, 18 years) for their histologic preparation and staining of tissue.

**Disclosures of Conflicts of Interest: P.F.** No relevant conflicts of interest to disclose. **M.E.M.** No relevant conflicts of interest to disclose. **S.F.** No relevant conflicts of interest to disclose. **K.J.S.** No relevant conflicts of interest to disclose. **D.W.D.** No relevant conflicts of interest to disclose. **Z.K.W.** Financial activities related to the present article: none to disclose. Financial activities not related to the present article: Coeditor-in-Chief, Elsevier; Regional Editor, Wiley-Blackwell. Other relationships: none to disclose. **S.C.G.** No relevant conflicts of interest to disclose.

## References

1. Seppi K, Poewe W. Brain magnetic resonance imaging techniques in the diagnosis of parkinsonian syndromes. Neuroimaging Clin N Am 2010;20(1):29–55.
2. Nath U, Ben-Shlomo Y, Thomson RG, et al. The prevalence of progressive supranuclear palsy (Steele-Richardson-Olszewski syndrome) in the UK. Brain 2001;124(Pt 7):1438–1449.
3. Litvan I, Agid Y, Calne D, et al. Clinical research criteria for the diagnosis of progressive supranuclear palsy (Steele-Richardson-Olszewski syndrome): report of the NINDS-SPSP international workshop. Neurology 1996;47(1):1–9.
4. Stamelou M, de Silva R, Arias-Carrión O, et al. Rational therapeutic approaches to progressive supranuclear palsy. Brain 2010;133(Pt 6):1578–1590.
5. Williams DR, de Silva R, Paviour DC, et al. Characteristics of two distinct clinical phenotypes in pathologically proven progressive supranuclear palsy: Richardson's syndrome and PSP-parkinsonism. Brain 2005;128(Pt 6):1247–1258.
6. Steele JC, Richardson JC, Olszewski J. Progressive supranuclear palsy. A heterogenous degeneration involving the brain stem, basal ganglia and cerebellum with vertical gaze and pseudobulbar palsy, nuchal dystonia and dementia. Arch Neurol 1964;10:333–359.
7. Paviour DC, Price SL, Jahanshahi M, Lees AJ, Fox NC. Regional brain volumes distinguish PSP, MSA-P, and PD: MRI-based clinico-radiological correlations. Mov Disord 2006;21(7):989–996.
8. Fujishiro H, Ferman TJ, Boeve BF, et al. Validation of the neuropathologic criteria of the third consortium for dementia with Lewy bodies for prospectively diagnosed cases. J Neuropathol Exp Neurol 2008;67(7):649–656.
9. McKeith IG, Dickson DW, Lowe J, et al. Diagnosis and management of dementia with Lewy bodies: third report of the DLB Consortium. Neurology 2005;65(12):1863–1872.
10. Murray ME, Knopman DS, Dickson DW. Vascular dementia: clinical, neuroradiologic and neuropathologic aspects. Panminerva Med 2007;49(4):197–207.
11. Josephs KA, Dickson DW. Diagnostic accuracy of progressive supranuclear palsy in the Society for Progressive Supranuclear Palsy brain bank. Mov Disord 2003;18(9):1018–1026.
12. Dickson DW, Rademakers R, Hutton ML. Progressive supranuclear palsy: pathology and genetics. Brain Pathol 2007;17(1):74–82.
13. Ma Y, Hof PR, Grant SC, et al. A three-dimensional digital atlas database of the adult C57BL/6J mouse brain by magnetic resonance microscopy. Neuroscience 2005;135(4):1203–1215.
14. Haines DE. Neuroanatomy: an atlas of structures, sections, and systems. 7th ed. Philadelphia, Pa: Wolters Kluwer/Lippincott Williams & Wilkins, 2008.
15. Bancroft JD, Stevens A. Theory and practice of histological techniques. 4th ed. Edinburgh, NY: Churchill Livingstone, 1996;245–246.
16. Meadowcroft MD, Connor JR, Smith MB, Yang QX. MRI and histological analysis of beta-amyloid plaques in both human Alzheimer's disease and APP/PS1 transgenic mice. J Magn Reson Imaging 2009;29(5):997–1007.
17. Nabuurs RJ, Hegeman I, Natté R, et al. High-field MRI of single histological slices using an inductively coupled, self-resonant microcoil: application to ex vivo samples of patients with Alzheimer's disease. NMR Biomed 2010 Oct 19. [Epub ahead of print]
18. Meadowcroft MD, Zhang S, Liu W, et al. Direct magnetic resonance imaging of histological tissue samples at 3.0T. Magn Reson Med 2007;57(5):835–841.
19. Quattrone A, Nicoletti G, Messina D, et al. MR imaging index for differentiation of progressive supranuclear palsy from Parkinson disease and the Parkinson variant of multiple system atrophy. Radiology 2008;246(1):214–221.
20. Wallis LI, Paley MN, Graham JM, et al. MRI assessment of basal ganglia iron deposition in Parkinson's disease. J Magn Reson Imaging 2008;28(5):1061–1067.
21. Martin WR. Quantitative estimation of regional brain iron with magnetic resonance imaging. Parkinsonism Relat Disord 2009;15(Suppl 3):S215–S218.
22. Hallgren B, Sourander P. The effect of age on the non-haemin iron in the human brain. J Neurochem 1958;3(1):41–51.

23. Martin WR, Ye FQ, Allen PS. Increasing striatal iron content associated with normal aging. Mov Disord 1998;13(2):281–286.

24. Kraft E, Schwarz J, Trenkwalder C, Vogl T, Pfluger T, Oertel WH. The combination of hypointense and hyperintense signal changes on T2-weighted magnetic resonance imaging sequences: a specific marker of multiple system atrophy? Arch Neurol 1999;56(2):225–228.

25. Rutledge JN, Hilal SK, Silver AJ, Defendini R, Fahn S. Study of movement disorders and brain iron by MR. AJR Am J Roentgenol 1987; 149(2):365–379.

26. Youdim MB, Riederer P. The role of iron in senescence of dopaminergic neurons in Parkinson's disease. J Neural Transm Suppl 1993;40:57–67.

27. Götz ME, Double K, Gerlach M, Youdim MB, Riederer P. The relevance of iron in the pathogenesis of Parkinson's disease. Ann N Y Acad Sci 2004;1012:193–208.

28. Wypijewska A, Galazka-Friedman J, Bauminger ER, et al. Iron and reactive oxygen species activity in parkinsonian substantia nigra. Parkinsonism Relat Disord 2010;16(5):329–333.

29. Bartzokis G, Cummings JL, Markham CH, et al. MRI evaluation of brain iron in earlier- and later-onset Parkinson's disease and normal subjects. Magn Reson Imaging 1999; 17(2):213–222.

30. Atasoy HT, Nuyan O, Tunc T, Yorubulut M, Unal AE, Inan LE. T2-weighted MRI in Parkinson's disease; substantia nigra pars compacta hypointensity correlates with the clinical scores. Neurol India 2004;52(3):332–337.

31. Antonini A, Leenders KL, Meier D, Oertel WH, Boesiger P, Anliker M. T2 relaxation time in patients with Parkinson's disease. Neurology 1993;43(4):697–700.

32. Martin WR, Wieler M, Gee M. Midbrain iron content in early Parkinson disease: a potential biomarker of disease status. Neurology 2008;70(16 Pt 2):1411–1417.

33. Zecca L, Youdim MB, Riederer P, Connor JR, Crichton RR. Iron, brain ageing and neurodegenerative disorders. Nat Rev Neurosci 2004;5(11):863–873.

34. Levenson CW, Tassabehji NM. Iron and ageing: an introduction to iron regulatory mechanisms. Ageing Res Rev 2004;3(3): 251–263.

35. Gelman BB. Iron in CNS disease. J Neuropathol Exp Neurol 1995;54(4):477–486.

36. Dexter DT, Carayon A, Javoy-Agid F, et al. Alterations in the levels of iron, ferritin and other trace metals in Parkinson's disease and other neurodegenerative diseases affecting the basal ganglia. Brain 1991;114(Pt 4):1953–1975.

37. Kaneko Y, Kitamoto T, Tateishi J, Yamaguchi K. Ferritin immunohistochemistry as a marker for microglia. Acta Neuropathol (Berl) 1989;79(2):129–136.

38. Ahmed Z, Shaw G, Sharma VP, Yang C, McGowan E, Dickson DW. Actin-binding proteins coronin-1a and IBA-1 are effective microglial markers for immunohistochemistry. J Histochem Cytochem 2007;55(7): 687–700.